

Stability of an erodible bed in various shear flows

K.K.J. Kouakou^{1,2} and P.-Y. Lagr e^{2,a}

¹ Laboratoire de M canique, Universit  de Cocody, Abidjan, C te d'Ivoire

² Laboratoire de Mod lisation en M canique, U.M.R. CNRS 7607, Universit  Pierre et Marie Curie, Bo te 162, 4 place Jussieu, 75252 Paris Cedex 05, France

Received 5 October 2005 / Received in final form 25 May 2005

Published online (Inserted Later) –   EDP Sciences, Societ  Italiana di Fisica, Springer-Verlag 2005

Abstract. The 2D laminar quasi-steady asymptotically simplified and linearized flow with a simplified mass transport of sediments is solved over a slowly erodible bed in various laminar basic shear flow (steady, oscillating or decelerating). The simplified mass transport equation includes the two following phenomena: flux of erosion when the skin friction goes over a threshold value, and a non local effect coming either from an inertial effect or from a slope effect. It is shown that the bed is always unstable for small wave numbers. Examples of long time evolution in various shear r gimes are presented, wave trains of ripples are created and merge into a unique bump. This coarsening process is such that the maximum wave length obeys a power law with time.

PACS. 45.70.-n Granular systems – 47.15.Cb Laminar boundary layers – 45.70.Qj Pattern formation

1 Introduction

Understanding how water or air creates ripples on sand or sediments is a very important environmental problem. Widely different wave lengths are involved from small ripples on the beach (either in the wet or dry sand) to dune formation in desert or mega ripples in sea. A large literature refers to this problem since du Boys in 1879, Exner in 1925, and Bagnold in the 40's up to now, as ripples on Mars may be an evidence of water on this planet [1].

These erosion/sedimentation problems have been solved by various techniques with various approaches. These problems may be seen from a practical point of view with direct application in costal engineering. Yang [2], Freds e and Deigaard [3], and Nielsen [4] give the state of the art for this very complex problem linking various physical aspects at different scales (from the grain diameter to the sea depth!).

Experimental setup have been constructed to study how ripples (of sand or beads) appear and grow in a flow of water. Typical experimental setups are oscillating annular cells (Sherer et al. [5], Rousseaux et al. [6,7]), uniformly rotating cell (Charru et al. [8,9], Kruelle et al. [10]) uniformly rotating disk ([11,12]) or stopping a disk which was uniformly rotating (Caps [13], here the shear is due to the fact that the soil is stopped and the flow continues to rotate). The flow is characterized by the shear at the wall which makes the soil move. The observed ripples are of centimetric size. It is observed that as time increases the wave length of the ripple increases. As the ripple increase in size and length, vortex appear in the lee side: before it

was the “rolling grain r gime”, after it is the “vortex ripple r gime”. When time increases more and more, there is less and less ripples: this is the coarsening of the ripples. It takes a long time (weeks, months?) to observe this coarsening.

This is an interacting problem between the deformable soil and the flow. On the first hand, to understand the flow it self, the ripples may be fixed: the shape is given. Then, simplified (Rousseau et al. [7]) or complete Navier Stokes computations (direct numerical resolution with turbulent models) may be done over the given ripples (Barr and Slinn [14], Andersen et al. [15], Andersen and Freds e [16,17] or Scandura et al [18]).

On the other hand, the relation between the shear and the flux of sediments is investigated (Charru et al. [9,8], Loiseleux et al. [19]). This study of the early stages is not simple. The first difficult problem is to measure the value of shear stress above which sediments are entrained. The second is to measure the sediment flux as a function of the shear stress. So, if appropriate experimental results for validation are still lacking, a lot of effort is done to measure the threshold value and the flux relation.

Coupling the flow and the soil variation allows computation of linear stability of the erodible bed. This has been done by Charru et al. [8], in the case of constant shear and slope effect in the flux relation, by Fowler [20] nearly in the laminar same case (though presented as turbulent), by Valance and Langlois [21] in the case of convective effect in the flux relation (this is similar to our analysis). From an experimental point of view, it is not simple to measure the first unstable wave length. Oscillating cases have been done by Mei and Yue [22] with a linear stability

^a e-mail: pyl@ccr.jussieu.fr

theory with $A/\lambda = 0(1)$ (A amplitude of the oscillation, λ wave length). The case of large values of A/λ has been examined by Gerkema [23] as well, our analysis is in fact similar to his analysis and makes it more general because applied to other régimes.

Previous studies where laminar. Komorova and Hulsher [24], Sumer and Bakioglu [25], and Richards [26] take into account turbulence, they have to model the turbulent viscosity.

The ripples of sand in air seem to be governed by a completely different mechanism from reptation saltation (Andreotti [27]) which does not involve fluid mechanics (Valance and Rioual [28], Balmforth et al. [29]), nevertheless fields of dunes are governed again by an interaction of the fluid and the transport of grains (Kroy et al. [30] and Sauerman et al. [31], Andreotti et al. [32]).

Finally, we notice that some studies use simplified physical models to compute the flow and the ripples evolution (Andersen [32], Nishimori et al. [33]). Rousseaux et al. [6] suggest that a Cahn-Hilliard model (Bray [34]) may give a prediction of coarsening for ripples.

We simulate this phenomena with a simple model for both the flow and the soil. Instead of using an amplitude model equation we want to use model equations coming from mechanics. The first difficulty consists in computing the flow which is unsteady and turbulent in the nature, but which may be considered as laminar in most experiments. Our model will consider quasi steady laminar perturbations of a slowly varying basic flow. An asymptotical approach allows to obtain a linearised solution for the flow over the ripples. This approach is done in a framework which allows boundary layer separation. This is done because it has been observed that the ripples produce vortices in their lee side. So, we focus on configurations of flow which describe boundary layer separation (the so called “triple deck”, which is here in fact a “double deck”).

The second difficulty consists in computing the flow of sand. The sand may “creep” (bed load transport), or “fly”, or may be suspended in the fluid. This modifies the viscosity and density of the flow. Our model will consider different simple relations between the flux of sand and the shear stress from the flow.

We present a stability theory valid for different cases of flow which is a generalization of other cases found in literature. The basic state is a flat erodible bed with a shear flow. Either a steady established flow, an oscillating one, or a decelerated one will be considered. The questions are about the linear stability of the configuration, and about the non linear long time evolution of the bed form. We then observe coarsening of the waves an fit a power law.

We first remind the equations of the full coupled problem (Sect. 2) and the first simplifications for the flow and for the granular material. We present the simple basic régimes: they reduce near the soil to a shear flow (Sect. 3). We focus on the small perturbations of this flow in Section 4. The linear stability is then discussed (Sect. 5). Finally we present a long time evolution (Sect. 6) of the erodible bed leading to the coarsening of wave length.

2 The coupled problem

2.1 The flow

We consider a steady or unsteady laminar incompressible Newtonian flow. We suppose that the viscosity and density remain constant in the flow. An initial boundary layer is developing, δ is its thickness, U_0 is the velocity far from the soil. The Reynolds number $Re_\delta = \frac{U_0\delta}{\nu}$ is supposed large enough to use an asymptotical approach. In fact the slope of the velocity at the surface U_0/δ will be the pertinent parameter (we note it U'_0 , this is often called $\dot{\gamma}$). The Reynolds number is in fact $Re_\delta = \frac{U'_0\delta^2}{\nu}$. We will specialise the boundary layer in Section (3). Knowing the instantaneous soil shape the problem is to find the velocity near the soil, more exactly the skin friction $\tau = \mu\partial_y u$ from the Navier Stokes equations. Using δ as length scale, $y = \delta\bar{y}$, $x = \delta\bar{x}$, $u = U_0\bar{u}$, and $t = (\delta^2/\nu)\bar{t}$. The Navier Stokes equations are (Rousseaux et al. [7]):

$$\frac{\partial\bar{u}}{\partial\bar{x}} + \frac{\partial\bar{v}}{\partial\bar{y}} = 0, \quad (1)$$

$$\frac{1}{Re_\delta} \frac{\partial(\bar{u}, \bar{v})}{\partial\bar{t}} + (\bar{u}, \bar{v}) \cdot \bar{\nabla}(\bar{u}, \bar{v}) = -\bar{\nabla}\bar{p} + \frac{1}{Re_\delta} \bar{\nabla}^2(\bar{u}, \bar{v}). \quad (2)$$

Here we will concentrate to the case of small perturbations of the soil’s surface, and we will see that asymptotic analysis allows an analytical resolution. The boundary conditions are the no slip flow at the upper surface of the soil described by $\bar{y} = f$.

2.2 The erodible bed

Due to the movement of sand or sediment, the upper surface of the soil ($y = f(x, t)$) changes according to the mass conservation. To solve the mass conservation of sediments

$$\frac{\partial f}{\partial t} = -\frac{\partial q}{\partial x}, \quad (3)$$

one has to know the relation between the flux q and the fluid flow. This depends on a lot of factors. In the literature (Yang [2], Nielsen [4], Fredsøe and Deigaard [3], ...) the final relation is mostly that q is function of the skin friction τ . The adimensionalised skin friction is denoted as the Shield number $\theta = \frac{\tau}{(\rho_s - \rho)gd}$; ρ and ρ_s are fluid and particle density ($s = \rho_s/\rho$), respectively, d is average particle diameter, and g is gravity. There is a threshold value τ_s (or critical Shield θ_s) above which the sediments are entrained, a power law is often used:

$$q_s \propto (\theta)^a (\theta - \theta_s)^b, \quad \text{with } \theta > \theta_s.$$

Coefficients a, b depend on the modelling. Du Boys [35] law corresponds to $a = b = 1$; Charru and Mouilleron-Arnould [8] law, issued from resuspension theory, corresponds to $a = 0, b = 3$; Sumer and Bakioglu [25] use $a = 1/2, b = 1$; Blondeaux [36] uses $a = 0, b = 4.28$; Peter-Meyer (see Fredsøe and Deigaard [3]) use $a = 0, b =$

3/2. Those different values correspond to various specific hypotheses, in various laminar or turbulent flows, in air or in water.

In fact, we use a linearized version just above the threshold: $q_s \propto \tau - \tau_s$. Furthermore, there is a gravity effect which induces a correction in the threshold value depending on the slope of the soil. It is proportional to the inverse of the tangent of the static friction angle ϕ_s . If $\tau > \tau_s + \Lambda \frac{\partial f}{\partial x}$ there is a flux, else there is no flux. Hence, we define a saturated flux as:

$$q_s = Q_0 \varpi \left(\frac{\tau - \tau_s - \Lambda \frac{\partial f}{\partial x}}{\rho(s-1)gd} \right), \quad (4)$$

where $\varpi(x) = x$ if $x > 0$, else $\varpi(x) = 0$. The expressions of τ_s , Q_0 and Λ are mainly in the literature:

$$\begin{aligned} \tau_s &= \theta_s \rho g (s-1) d, \\ Q_0 &= 8 \sqrt{g(s-1)d^3}, \\ \text{and } \Lambda &= \frac{\theta_s \rho g (s-1) d}{\tan(\phi_s)}. \end{aligned} \quad (5)$$

In an eolian context, Kroy et al. [30], Sauermann et al. [31] introduced an effect of inertia adding a term proportional to $\partial_x q$ (with $\Lambda = 0$), we may simplify their expression as:

$$l_K \frac{\partial q}{\partial x} + q = q_s \quad (6)$$

with l_K proportional to $\frac{1}{\bar{U}'_s}$ i.e. the inverse of the shear. With again $\Lambda = 0$, Andreotti et al. [37] simplified this expression as:

$$l_s \frac{\partial q}{\partial x} + q = q_s, \quad (7)$$

with a constant coefficient in front of $\partial_x q$. Assuming an equilibrium in the granular media modeled by a BCRE model, Valance and Langlois [21] proposed this same relation for water ripples.

Finally the slope of the ripple may be limited by an ‘‘avalanche’’ effect (at least a ‘‘slope effect’’). It means that at each time step:

$$\text{if } \left| \frac{\partial f}{\partial x} \right| > \frac{1}{\mu}, \text{ then } \left| \frac{\partial f}{\partial x} \right| = \frac{1}{\mu} \quad \text{and} \quad \int f dx = cste. \quad (8)$$

Mass is conserved during this process, and slope is limited. The problem is now to find τ and to test either equations (4, 6), or (7), and (8).

3 Basic flow

The basic configuration is a bidimensional flow over a flat soil. Curvature and gap effects in circular cells are neglected. The flow is laminar. Near the wall, any velocity profile reduces to a pure shear flow (Fig. 1). The basic adimensionalised velocity is:

$$\bar{u} = \bar{U}'_s \bar{y}. \quad (9)$$

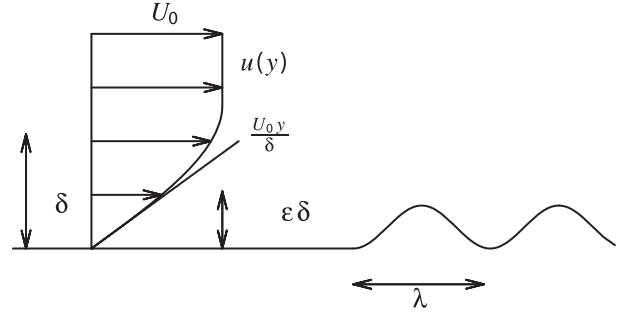


Fig. 1. Any velocity profile is linear near the wall. λ is a typical length. $H = \epsilon\delta$ is the typical height.

Typical examples are an oscillating flow, or a moving tank with an impulsively stopped bottom or a Blasius boundary layer. In the next subsections we will show that the steady case corresponds to $\bar{U}'_s = 1$, the oscillating case corresponds to $\bar{U}'_s = \cos(2\pi\bar{t})$, and the decelerated case to $\bar{U}'_s = \bar{t}^{-1/2}$. The shear itself is denoted $U'_0 = U_0/\delta$.

3.1 Steady basic flow

If we consider a Blasius boundary layer, near the wall, the profile is linear (Schlichting [38]):

$$u \simeq 0.33U_0 \frac{y}{\delta} \quad (10)$$

with $\delta = (LR_L^{-1/2})$ so that we obtain (9) with $\bar{U}'_s = 0.33$. We may as well imagine a flow in a channel with a developed half Poiseuille profile, the parabolic velocity profile being linear near the wall. The analysis of Fowler [20] of a turbulent flow with a mean equivalent viscosity leads in fact to this analysis.

3.2 Oscillating basic flow

In the frame of the wall, the basic flow is solution of:

$$\frac{\partial}{\partial t} u = -\frac{d}{\rho dx} p + \nu \frac{\partial^2}{\partial y^2} u. \quad (11)$$

The oscillating velocity $U_0 \Re[\exp(-i\Omega t)]$ is imposed at ‘‘infinity’’, far from the bottom where $u(y=0, t) = 0$. The solution is classical (Schlichting [38]) and after a change of phase in the time, near the wall:

$$u \simeq U_0 \frac{y}{\delta} e^{-i\Omega t} + \dots \quad (12)$$

so that we obtain (9) with $\bar{U}'_s = \cos(2\pi\bar{t})$, with time scaled with $f^{-1} = 2\pi\Omega^{-1}$. The scale of the boundary layer $\delta = (\nu/\Omega)^{1/2}$.

3.3 Decelerated basic flow

In the frame of the wall, the basic flow is again the solution of equation (11) (Rayleigh problem) with U_0 the

constant velocity at “infinity”, far from the bottom and $u(y = 0, t) = 0$:

$$u \simeq U_0 \frac{y}{\sqrt{\pi E \nu t}} + \dots \quad (13)$$

so that we obtain (9) with $\bar{U}'_S = 1/\sqrt{\bar{t}}$, $\delta = (\pi \nu T^*)^{1/2}$ were $T^* = h_0^2/\nu$ is the chosen time scale (h_0 is the water depth, which is supposed larger than δ).

4 Perturbation of the basic flow

As mentioned in the literature, the ripples are of small aspect ratio. Let then consider a bump of thickness $H = \varepsilon \delta$ and of length $\lambda \gg \delta$ (Fig. 1). In the sublayer of relative thickness ε (compared to the uniform boundary layer thickness δ), and longitudinally stretched of a factor λ/δ we may develop (1–2) using $\tilde{y} = \varepsilon^{-1} \bar{y} = \frac{y}{\varepsilon \delta}$ and $\tilde{x} = \frac{\delta}{\lambda} \bar{x} = \frac{x}{\lambda}$. Perturbations of velocity must be of order ε , in order to reobtain far upstream of the bump: $\tilde{u} = \bar{U}'_S \tilde{y}$. The harder simplified problem to solve is the simplified problem which has the maximal number of terms in the equations. This is the “least possible degeneracy” (Van Dyke [39], p. 86, or Darrozès [40]). So, to have a problem with the maximum number of terms, including pressure, convective terms and a viscous term, there should be a relation between λ and δ :

$$\lambda = \varepsilon^3 \delta R_\delta. \quad (14)$$

Therefore with $\bar{u} = \varepsilon \tilde{u}$, $\bar{v} = (\delta/\lambda) \varepsilon \tilde{v}$, and $\bar{p} = \varepsilon^2 \tilde{p}$, and if we take the time scale to be the time scale of the oscillating flow $\bar{t} = \tilde{t}$, we have:

$$\varepsilon^2 \frac{\partial}{\partial \tilde{t}} \tilde{u} + \tilde{u} \frac{\partial}{\partial \tilde{x}} \tilde{u} + \tilde{v} \frac{\partial}{\partial \tilde{y}} \tilde{u} = -\frac{\partial}{\partial \tilde{x}} \tilde{p} + \frac{\partial^2}{\partial \tilde{y}^2} \tilde{u} + \varepsilon^2 \frac{\partial^2}{\lambda^2} \frac{\partial^2}{\partial \tilde{x}^2} \tilde{u}, \quad (15)$$

and $-\frac{\partial}{\partial \tilde{y}} \tilde{p} = O(\varepsilon^2)$. So that, as $\varepsilon \rightarrow 0$, the problem is quasisteady, and we obtain a “boundary layer” equation for \tilde{u} which will be (Eq. (17)).

4.1 Notes on the scalings

We note (as $\varepsilon \rightarrow 0$) that the second order partial longitudinal derivative is not present. It is because the transverse scale is smaller than the longitudinal one. Using the same scale in both directions $x = \lambda_v \hat{x}$ and $y = \lambda_v \hat{y}$, (i.e. $\lambda = \varepsilon \delta = \lambda_v$ in Eq. (15)) we have $\lambda_v = \sqrt{\nu/(U_0/\delta)}$ and equation (2), for \hat{u} is:

$$\varepsilon^2 \frac{\partial \hat{u}}{\partial \hat{t}} + \hat{u} \frac{\partial \hat{u}}{\partial \hat{x}} + \hat{v} \frac{\partial \hat{u}}{\partial \hat{y}} = -\frac{\partial}{\partial \hat{x}} \hat{p} + \frac{\partial^2}{\partial \hat{y}^2} \hat{u} + \frac{\partial^2}{\partial \hat{x}^2} \hat{u}.$$

Again, the problem is steady. This scale is called the “viscous scale” (Charru et al. [8]), it is supposed very small. Nevertheless, looking at a large scale ($\hat{x} = X \tilde{x}$), small aspect ratio perturbation ($\hat{y} = X^{1/3} \tilde{y}$, $\hat{u} = X^{1/3} \tilde{u}$, $\hat{p} = X^{2/3} \tilde{p}$, and $\hat{v} = X^{-1/3} \tilde{v}$) of this equation gives:

$$\tilde{u} \frac{\partial}{\partial \tilde{x}} \tilde{u} + \tilde{v} \frac{\partial}{\partial \tilde{y}} \tilde{u} = -\frac{\partial}{\partial \tilde{x}} \tilde{p} + \frac{\partial^2}{\partial \tilde{y}^2} \tilde{u} + X^{-4/3} \frac{\partial^2}{\partial \tilde{x}^2} \tilde{u}.$$

So that we will recover (Eq. (17)) for scales larger than λ_v .

In fact we are in the Triple Deck theory (Neiland [41], Stewartson and Williams [42], Smith [43], Sychev et al. [44]), and Gajjar and Smith [45], Bowles and Smith [46]). This set of equations is known to be relevant to describe boundary layer separation. More precisely, we are in the framework of Double Deck Smith [43]. We focus on the case with no perturbations of the Upper Deck (no retroaction of the ideal fluid). This means that perturbations of pressure induced by the deflection of the streamlines in the Upper Deck (of order $\frac{\varepsilon \delta}{\lambda \varepsilon^3 \delta}$) are smaller than the perturbation of pressure in the Lower Deck (of order ε^2) (Smith et al. [47]). In the Blasius case, this means that $\varepsilon \ll R_L^{-1/8}$.

In complete Triple Deck, time should then be scaled by ε^2 compared to the time scale of the basic flow in this lower layer. But this is not relevant here because this introduces a smaller time scale than the one coming from the flow (i.e. $1/\Omega$ in the oscillating case). Furthermore, the time of variation of the soil is itself very long compared to the oscillation period.

4.2 Equations

Steady and unsteady cases follow the same equations, the problem in the “Lower Deck” is simply:

$$\frac{\partial}{\partial \tilde{x}} \tilde{u} + \frac{\partial}{\partial \tilde{y}} \tilde{v} = 0, \quad (16)$$

$$\tilde{u} \frac{\partial}{\partial \tilde{x}} \tilde{u} + \tilde{v} \frac{\partial}{\partial \tilde{y}} \tilde{u} = -\frac{d}{d\tilde{x}} \tilde{p} + \frac{\partial^2}{\partial \tilde{y}^2} \tilde{u}. \quad (17)$$

It means that near the wall there exist scales such that a non linear problem (with convection, diffusion and pressure gradient) has to be solved. Solving numerically this problem may lead to boundary layer separation: there is a small thin vortex in the lee side of the bump. Boundary conditions are no slip condition on the bottom:

$$\tilde{u}(\tilde{x}, \tilde{y} = \tilde{f}(\tilde{x})) = 0, \quad \tilde{v}(\tilde{x}, \tilde{y} = \tilde{f}(\tilde{x})) = 0. \quad (18)$$

The matching between the top of the Lower Deck ($\tilde{y} \rightarrow \infty$) and the bottom of the boundary layer ($\tilde{y} \rightarrow 0$) gives:

$$\lim_{\tilde{y} \rightarrow \infty} (\varepsilon \tilde{u}(\tilde{x}, \tilde{y})) = \bar{U}'_S \tilde{y} \quad \text{i.e.} \quad \tilde{u}(\tilde{x}, \tilde{y} \rightarrow \infty) = \bar{U}'_S \tilde{y}. \quad (19)$$

The latter means that the incoming velocity is linear, this means that upstream we recover the boundary layer profile:

$$\tilde{u}(\tilde{x} \rightarrow -\infty, \tilde{y}) = \bar{U}'_S \tilde{y}, \quad \tilde{v}(\tilde{x} \rightarrow -\infty, \tilde{y}) = 0. \quad (20)$$

4.3 Linearisation: law between the topography and the skin friction

The unperturbed solution of (16–17) is simply:

$$\tilde{u} = \bar{U}'_S \tilde{y}, \quad \tilde{v} = 0, \quad \tilde{p} = 0.$$

This means that at the small longitudinal scale, the boundary layer thickness does not evolve and the velocity profile remains linear near the wall. The linearised solution of (16–17) around this shear profile in Fourier space is straightforward and leads to (Ai is the Airy function):

$$\tilde{\tau} = \bar{U}'_S + \bar{U}'_S FT^{-1}[FT[\tilde{f}](3Ai(0))(-ik\bar{U}'_S)^{1/3}] + \dots \quad (21)$$

This relation (21) gives the final response of the fluid: it links the perturbation of the shear stress to the topography change. This final relation will be used for the linear stability analysis as well as for the numerical simulations.

Going back in physical variables gives for a bump of length of order λ and of height of order H :

$$\tau = \mu U'_0 (\bar{U}'_S (1 + (\frac{U'_0}{\nu \lambda})^{1/3} H \tilde{c})),$$

$$\text{with } \tilde{c} = FT^{-1}[FT[\tilde{f}]3Ai(0)(-i2\pi\tilde{k}\bar{U}'_S)^{1/3}] \quad (22)$$

\tilde{c} is a numerical coefficient depending of the exact adimensionalised shape, the height H is supposed to be smaller than δ . The function of time \bar{U}'_S is a number of order one. If $(\frac{U'_0}{\nu \lambda})^{1/3} H$ is of order one this is equivalent to formula (14). Comparisons of formula (22) with Navier Stokes computations and full non linear equations (16–17) has been done by Kouakou and Lagrée [48] and Kouakou et al. [49]. It gives good results of boundary layer separation.

5 Linear stability of the bed

5.1 Steady case

The shear stress function of the topography change is now coupled to the adimensional version of (4),

$$\tilde{q}_s = \varpi \left(\tilde{\tau} - \tilde{\tau}_s - \tilde{\Lambda} \frac{\partial \tilde{f}}{\partial \tilde{x}} \right). \quad (23)$$

Either the flux is always saturated and

$$\tilde{q} = \tilde{q}_s, \quad (24)$$

or the inertial effect is taken into account with a variable coefficient (6)

$$\frac{\tilde{l}_K}{\bar{U}'_S} \frac{\partial \tilde{q}}{\partial \tilde{x}} + \tilde{q} = \tilde{q}_s, \quad (25)$$

or the inertial effect is taken into account with a constant coefficient (7)

$$\tilde{l}_s \frac{\partial \tilde{q}}{\partial \tilde{x}} + \tilde{q} = \tilde{q}_s, \quad (26)$$

where $\tilde{\tau}_s$, $\tilde{\Lambda}$, \tilde{l}_K , and \tilde{l}_s are constants. In practice, in the sequel, we do not mix the effect of inertia $\frac{\partial \tilde{q}}{\partial \tilde{x}}$ and the avalanche (or slope) effect $\frac{\partial \tilde{f}}{\partial \tilde{x}}$, so in (25 and 26) $\tilde{\Lambda}$ is zero in \tilde{q}_s . The bed form evolution (3) with a suitable adimensionalisation is:

$$\frac{\partial \tilde{f}}{\partial \tilde{t}} = -\eta \frac{\partial \tilde{q}}{\partial \tilde{x}}, \quad (27)$$

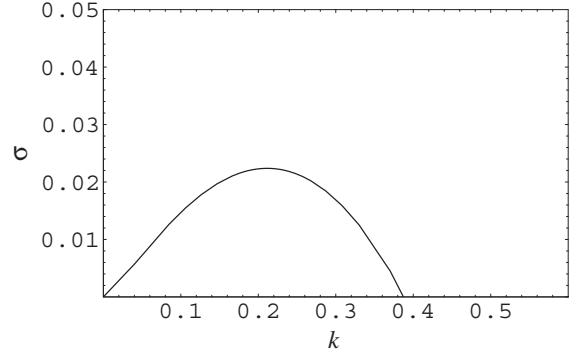


Fig. 2. Constant shear, $\bar{U}'_S = 1$, amplification factor σ as function of number k , case (4 or 24, and 28) with $\tilde{\Lambda} = 1$ (most unstable wave $k_{max} = 0.21$, $\sigma_{max} = 0.02$), decreasing $\tilde{\Lambda}$ increases the cut off value of k .

where η represents the ratio of the hydrodynamic scale versus the bed evolution one. In practice this arises only when \bar{U}'_S is not constant. When \bar{U}'_S is constant, the time scale is such that $\eta = 1$. We introduce a long time $\tilde{t}_1 = \eta \tilde{t}$. This allows to compute the temporal stability of an erodible bed with \bar{U}'_S given. Looking for normal modes $\tilde{f} = e^{(\sigma+i\omega)\tilde{t}_1} e^{-ik\tilde{x}}$, we obtain the perturbation of the skin friction (Eq. (21)) and with the suitably adimensionalised version of flux relation (Eqs. (24) or (25) or (26)), we obtain σ as a function of the mode k . We note that there exist a uniform flux:

$$\tilde{q}_0 = \bar{U}'_S - \tilde{\tau}_s.$$

With $\tilde{q}_0 > 0$, the linear stability analysis is valid as long $\tilde{\tau} - \tilde{\tau}_s > 0$. The amplification factor σ is positive for small k (with Eq. (4)):

$$\sigma + i\omega = \frac{3^{1/3}}{\Gamma(\frac{2}{3})} \left(\frac{1}{2} + \frac{i\sqrt{3}}{2} \right) k^{4/3} - \tilde{\Lambda} k^2. \quad (28)$$

Unstability occurs only for long waves (Fig. 2). If the slope effect is removed ($\tilde{\Lambda} = 0$ in Eq. (4)), all waves are amplified ($\sigma = 0.53k^{4/3}$ and $\omega = 0.92k^{4/3}$). The same arises for the case with saturation effect (Eqs. (7) or (6) here identical), there is unstability only for long waves (Fig. 3).

Figure 4 gives an interpretation of the unstability, a wavy profile has an excess of skin friction $\tilde{\tau} - \bar{U}'_S$ that is maximal just before the crest. The flux is decomposed in a uniform flux \tilde{q}_0 plus a perturbation which is $\tilde{\tau} - \bar{U}'_S$. This latter contribution erodes the crest and displaces the matter down stream.

5.2 Oscillating case

5.2.1 Averaging the flux relation

The oscillating time scale is supposed smaller than the time of growth of the structures. We have again (27) with η ratio of the oscillating time by the bed evolution one.

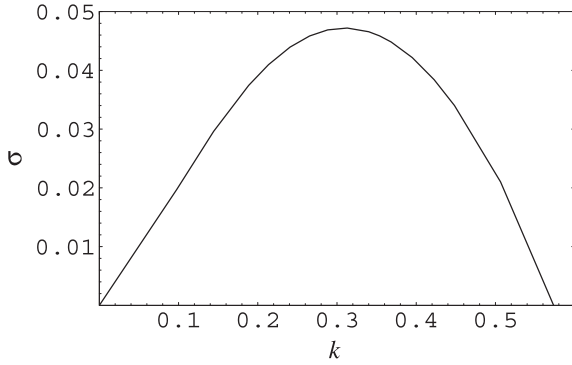


Fig. 3. Constant shear, $\bar{U}'_S = 1$, amplification factor σ as function of number k , case (7 or 25 or 26) with $\bar{l}_K = 1$ (most unstable wave $k_{max} = 0.31$, $\sigma_{max} = 0.047$), decreasing \bar{l}_K increases the cut off value of k .

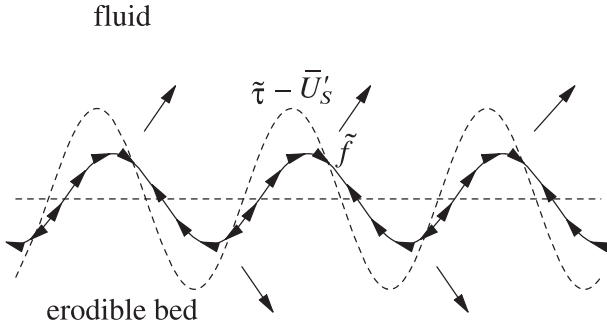


Fig. 4. A wavy profile (bold line, \tilde{f}) has a perturbation of skin friction (dashed line, $\tilde{\tau} - \bar{U}'_S$) in advance of phase. When it is positive, the matter is moved down stream (small arrows on the profile), when it is negative, it is in opposite direction. The result is an increase of the wave and a displacement in the stream direction (large inclined arrows).

We define a mean value $\langle \cdot \rangle = \int_0^1 \cdot d\bar{t}$ during an oscillating cycle. Introducing a multiscale analysis: $\bar{t}_0 = \bar{t}$ is the short time, and $\bar{t}_1 = \eta \bar{t}$ is the long time. Let split $\tilde{f} = \tilde{f}_0(\bar{t}_0, \bar{t}_1) + \eta \tilde{f}_1(\bar{t}_0, \bar{t}_1) + \dots$ and write $\tilde{q} = \tilde{Q} + \tilde{q}'$. \tilde{Q} is defined as the mean value during the current cycle $\tilde{Q} = \langle \tilde{q} \rangle$ and $\langle \tilde{q}' \rangle = 0$. So, as the time derivative is: $\frac{\partial}{\partial \bar{t}} = \frac{\partial}{\partial \bar{t}_0} + \eta \frac{\partial}{\partial \bar{t}_1}$, the mass conservation equation degenerates:

$$\frac{\partial \tilde{f}_0}{\partial \bar{t}_0} = 0,$$

i.e. the topology is quasisteady at the short time scale. We define $\tilde{F}_0(\bar{t}_1) = \tilde{f}_0(\bar{t}_0, \bar{t}_1)$. At the long time scale:

$$\frac{\partial \tilde{F}_0}{\partial \bar{t}_1} + \frac{\partial \tilde{f}_1}{\partial \bar{t}_0} = -\frac{\partial \tilde{q}}{\partial \bar{x}}.$$

With the decomposition of q :

$$\frac{\partial \tilde{f}_1}{\partial \bar{t}_0} = \left(-\frac{\partial \tilde{q}'}{\partial \bar{x}} \right) + \left(-\frac{\partial \tilde{Q}}{\partial \bar{x}} - \frac{\partial \tilde{F}_0}{\partial \bar{t}_1} \right).$$

In order to solve the problem at order one, the secular term: $(-\frac{\partial \tilde{Q}}{\partial \bar{x}} - \frac{\partial \tilde{F}_0}{\partial \bar{t}_1})$ must be 0:

$$\frac{\partial \tilde{F}_0}{\partial \bar{t}_1} = -\frac{\partial \langle \tilde{q} \rangle}{\partial \bar{x}}.$$

This means that we can take the mean value of q to deal with the long time evolution of the bed.

5.2.2 stability

During a cycle the ripples do not change at first order, the time of evolution of the topography is very slow compared to the oscillating time. The small short time perturbation of the soil is given by $\partial_{\bar{t}_0} \tilde{f}_1 = -\partial_{\bar{x}} \tilde{q}'$, where \tilde{q}' must be borned. So we estimate the mean value of the skin friction with a “frozen” soil from Eq. (21) during a cycle (note $\langle \bar{U}'_S \rangle = 0$, and we use \tilde{f} which is in fact \tilde{F}_0):

$$\langle FT[\tilde{\tau}] \rangle = -3Ai(0) \frac{i\Gamma(\frac{1}{6})}{8\sqrt{\pi}\Gamma(\frac{2}{3})} (k)^{1/3} FT[\tilde{f}],$$

$\langle \tilde{\tau} \rangle$ and \tilde{f} are out of phase, the skin friction will induce the sand to move to the crests and out of the hollow (Fig. 7) without displacing the ripples. The mean value of the skin friction is real:

$$\int_0^1 -(-ik)FT[\tau]d\bar{t} = \frac{3^{1/3}\Gamma(\frac{1}{6})k^{4/3}TF[\tilde{f}]}{8\sqrt{\pi}\Gamma(\frac{2}{3})^2}, \quad (29)$$

the numerical value is $0.3087TF[\tilde{f}]$.

Putting the slope effect (24), the stability analysis gives:

$$\sigma = 0.3087k^{4/3} - \tilde{\Lambda}k^2, \quad \omega = 0, \quad (30)$$

this dispersion relation is real, there is no phase speed. There is a cut off frequency k_c . Stability for large k : $k > k_c$ and instability for $k < k_c$. See Figure 5. Taking a relation with an inertial effect depending on the actual value of the shear stress (25) with $\tilde{q}_s = \tau$ gives:

$$\sigma + i\omega = \langle -(-ik) \frac{\tilde{U}'_S 3Ai(0)(-ik)\bar{U}'_S)^{1/3}}{1 - \bar{l}_K(ik(\bar{U}'_S)^{-1})} \rangle, \quad (31)$$

which is real again ($\omega = 0$), and plotted in Figure 6. As for the steady case, long waves are unstable, in this oscillating case there is no phase velocity. The ripples do not move.

5.3 Decelerated case

In the previous section, the hydrodynamic time was smaller than the bed time evolution. If we look at a decelerated flow, generally no ripples are created. The time during which the flow exists is too short for ripples to grow. In some cases, this arises (Caps [13]). In order to describe this case, the time scale of the flow must be the same than the time scale of the bed. Taking the same

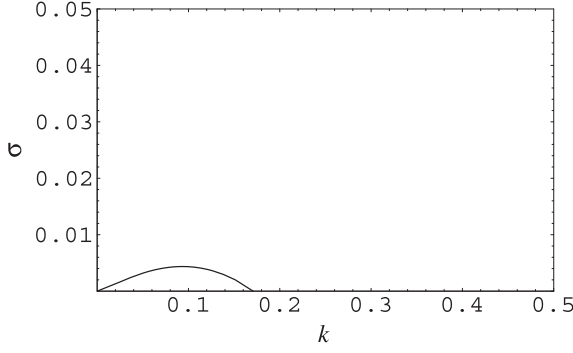


Fig. 5. Amplification factor function of wave number. Averaged oscillating case, $\Lambda = 1$ (most unstable wave $k_{max} = 0.09$, $\sigma_{max} = 0.0043$), case (4 and 30).

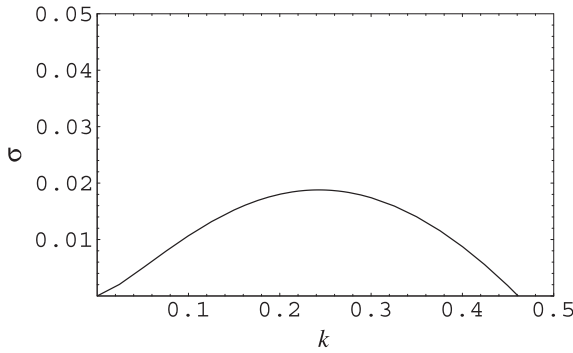


Fig. 6. Amplification factor function of wave number. Averaged oscillating case, $\tilde{l}_K = 1$ (most unstable wave $k_{max} = 0.24$, $\sigma_{max} = 0.019$) case (7 and 31).

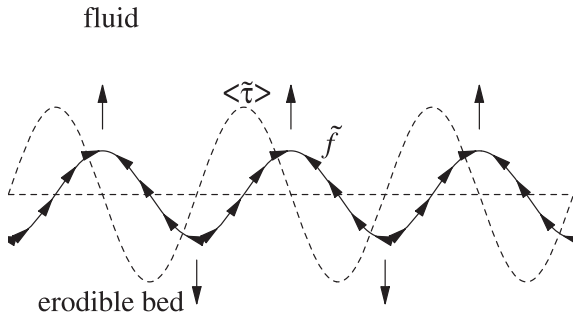


Fig. 7. A wavy profile (bold line, \tilde{f}) has a mean perturbation of skin friction (dashed line, $\langle \tilde{\tau} \rangle$) out of phase. When $\langle \tilde{\tau} \rangle$ is positive, the matter is moved from left to right (small arrows on the profile), when it is negative, it is in opposite direction. The result is an increase of the wave without displacement (large vertical arrows).

scale for the flow and the topology variation we have (in the case (24)):

$$\frac{\partial \tilde{f}_k}{\partial \tilde{t}} = (-3Ai(0)(-ik)(-ik)^{1/3} \tilde{t}^{-2/3} - \tilde{\Lambda} k^2) \tilde{f}_k. \quad (32)$$

Which may be solved for each Fourier mode k :

$$\log(\tilde{f}_k) = -9Ai(0)(-ik)(-ik)^{1/3} \tilde{t}^{1/3} - \tilde{\Lambda} k^2 \tilde{t}. \quad (33)$$

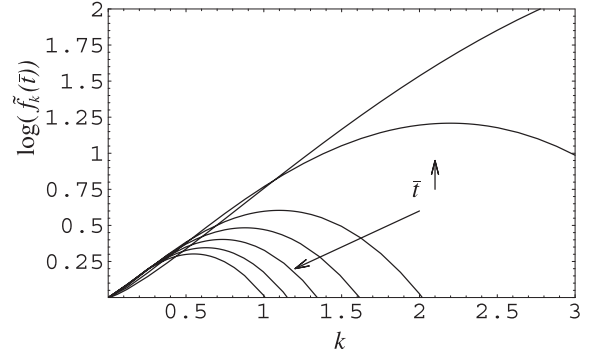


Fig. 8. Decelerated case $\tilde{\Lambda} = 1$ (24 and 33), plot of $\log(\tilde{f}_k(\tilde{t}))$ as function of k for various increasing times. As time increases, short waves are more and more stabilised.

Stability analysis now deals with $\log(\tilde{f}_k)$. In Figure 8 is displayed $\log(\tilde{f}_k)$ as function of k for various time. As time increases, the cut off frequency k_c decreases. Short waves are more and more stabilised.

5.4 Conclusion for stability analysis

As a conclusion for this section devoted to linear stability analysis, we observe that the qualitative behaviour is the same in every case: the long wave are unstable, the short wave are stabilised by the gravity or the inertia effect. In the oscillating case, there is no downstream propagation of the ripples.

The scale of the most unstable ripple is given by the flux relation itself either 4 or 7. In the “slope” case (4), Λ dictates the scale, in the “inertia” case (7), l_s dictates the scale, so, either,

$$\lambda = \left(\frac{\Lambda^3}{\rho^3 \nu^2 U_0'^4} \right)^{1/2}, \quad \text{or} \quad \lambda = l_s. \quad (34)$$

The time scale follows from the mass conservation, $T = \lambda H / Q_0$:

$$T = \left(\frac{\nu \lambda^4}{U_0' Q_0^3} \right)^{1/3}. \quad (35)$$

6 Examples of large time evolution

6.1 numerical method

The system is solved numerically using a fast Fourier transform ([50]). The non linearity of the problem is taken in real space and consists in the fonction ϖ that is zero under the threshold. The initial profile is a random small noise. We observe (see following figures) that the time for ripples to grow and to interact is very long. Therefore we solved the oscillating case with $\eta = 1$ (taking at each time step \tilde{t} the exact value of $\tilde{\tau}$). This is a simple way to tackle with the problem of the non linearity induced by ϖ . We obtain a coarsening in all the configurations.

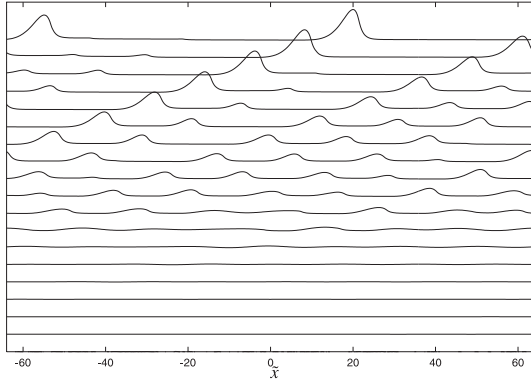


Fig. 9. Steady case, with (25) with $\bar{U}'_S = 1$, $\bar{l}_s = 1$. Spatio-temporal diagram ($t = 0, 20, 40, \dots$ from bottom to top). The flow is from left to right. Starting from a random small noise, structures emerge and merge.

6.2 Steady case

Starting from a random noise, the structures predicted by the linear theory appear. As time increases, the non linear stage is induced by the threshold function ϖ . The sinusoidal shape is transformed in a non symmetrical shape (see Fig. 9 a spatio temporal diagram). The ripples move from left to right. The ripple downstream of a larger one is eaten by it. This is due to the fact that the lee bumps experiment a smaller skin friction than the one upstream. As a result, there is less and less bumps in the computational domain: this is “coarsening”. Finally there is only one bump in the “box”. In Figure 10 is plotted the number of bumps which diminishes with time, whereas the bump height increases with time. The eight of the final bump saturates. The wave length λ_{max} (which corresponds to the distance between the bumps, and is inversely proportional to the number of bumps) increases. In Figure 11 is plotted this wave length for several simulation with various values of domain size, values of threshold τ_s and models (either 24 or 25). The large time behaviour is the same, this is due to the fact that at small wave length k the bump is large so the exact value of threshold does not matter anymore. Furthermore, as the wave length is small, Eqs. (24) or (25) are identical and reduce to

$$\tilde{q} = \tilde{\tau} + \dots$$

The wave length λ_{max} is plotted as function of t in Figure 11. A log-log plot suggest that λ_{max} is more or less proportional to time, it seems that: $\lambda_{max} \propto \bar{t}$.

6.3 Oscillating case

Starting again from a random noise, the structures predicted by the linear theory appear. As time increases, the non linear stage is induced by the threshold function ϖ . The sinusoidal shape is transformed in a symmetrical shape (right/ left, see Fig. 13) due to the symmetry of the flow. The ripples are steady and only move from one to the

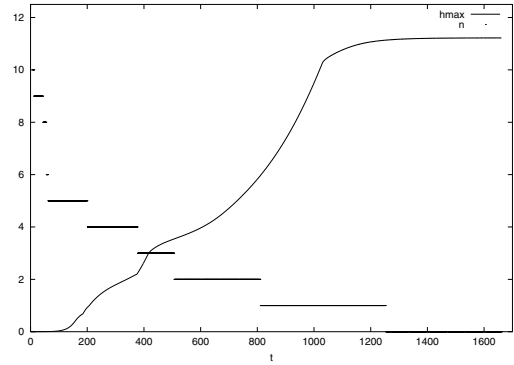


Fig. 10. Steady case $\bar{U}'_S = 1$, $\bar{l}_s = 1$, evolution of the maximum value and of the number of bumps in the domain versus time.

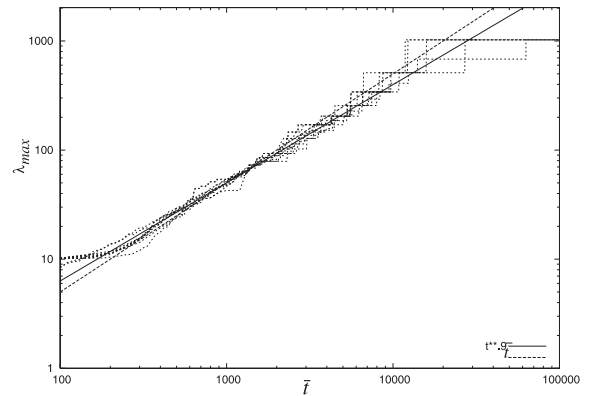


Fig. 11. Constant shear, the wave length of the structure scales with a power between $\bar{t}^{0.9}$ and \bar{t} .

other during the pairing process. Again, there is “coarsening”: less and less bumps are in the computational domain. Finally there is only one bump in the “box”. In Figure 12 the same is observed in the case of slope limitation (8). In Figure 14 is plotted the number of bumps which diminishes, whereas the bump height increases. The wave length λ_{max} increases. In Figure 15 is plotted this wave length for several simulations with various values of domain size, values of threshold τ_s and models (either 24 or 25). The large time behaviour is again the same. The wave length λ_{max} is plotted as function of t in Figure 15. A log-log plot suggest that is near a 2/3 power: $\lambda_{max} \propto t^{0.6}$ which is different from the steady case (Fig. 11).

6.4 Decelerated case

As already mentioned, the time to obtain the growth of ripples is long, here the time is borned (there exist a time at which $\bar{U}'_S = \tilde{\tau}_s$). So $\tilde{\tau}_s$ must be enough small. The final time of growth is a bit larger than the time at which $\bar{U}'_S = \tilde{\tau}_s$. In Figure 16 is a spatio-temporal diagram. As the effect of a bump is to increase the skin friction, there is an excess of $\tilde{\tau} - \tilde{\tau}_s$ that is only due to the crest of the ripple.

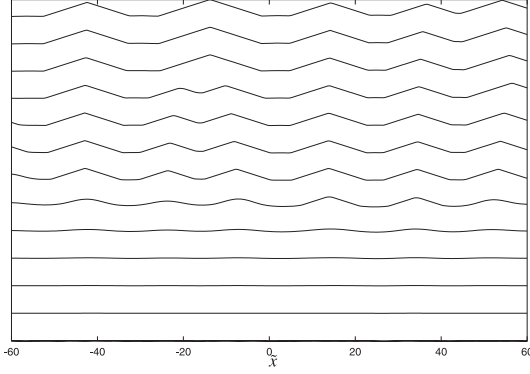


Fig. 12. Oscillating régime with (25) and slope limitation $V = 1$, $\frac{1}{\mu} = 0.05$, spatio-temporal diagram, time increases from bottom to top.

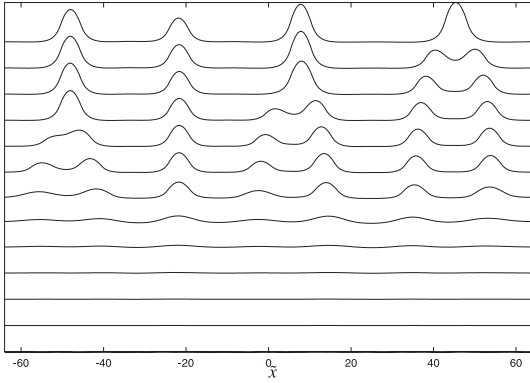


Fig. 13. Oscillating régime with (25), spatio temporal diagram, time increases from bottom to top. Ripples growth from a random noise and merge two by two.

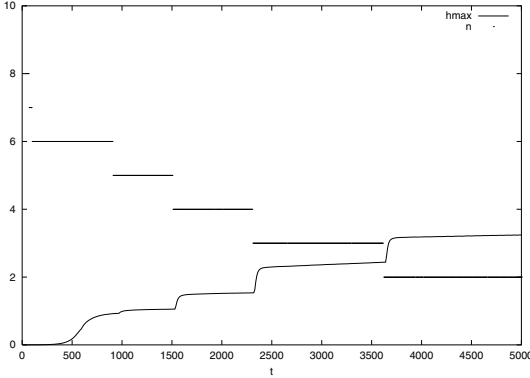


Fig. 14. oscillating case $\bar{U}'_S = \cos(\bar{t})$, $\bar{l}_K = 1$, evolution of the maximum height of the bumps, and number of bumps in the domain versus time.

6.5 Some experimental crude comparisons

First, in the case of constant shear, some orders of magnitude may be taken from Betat et al. [10] and [51], where the most unstable wave length is about 9 cm, and the order of magnitude of the wave growth is about $3 \times 10^{-3} \text{ s}^{-1}$ (for a shear with $U'_0 = 69 \text{ s}^{-1}$). Taking $\theta_s = 0.06$, $\phi_s = 30^\circ$, and numerical values from their experiment: $d = 95 \times 10^{-6} \text{ m}$, $s = 2.65$ gives a value of the most

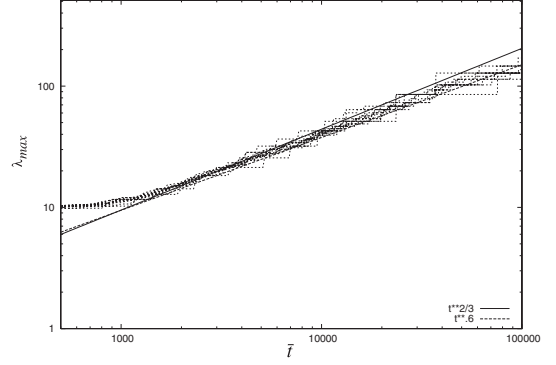


Fig. 15. Oscillating shear, the wave length of the structure scales with a power law between $\bar{t}^{0.6}$ and $\bar{t}^{2/3}$.

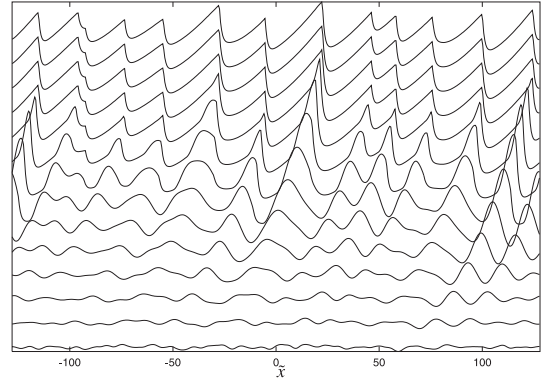


Fig. 16. Decelerated case with (26) $\bar{l}_s = 1$. Spatio-temporal diagram, time increases from bottom to top. There is a final steady bed because the shear stress is under the threshold.

unstable wave length (using Eqs. (28, 34) and Fig. 2):

$$\lambda^* \simeq 15 \text{ cm.}$$

The order of magnitude is correct (in increasing a bit θ_s , and decreasing a bit ϕ_s , we could obtain 9 cm). The order of magnitude of the wave growth is then about

$$\sigma^* = 1.2 \times 10^{-3} \text{ s}^{-1},$$

which is the order of magnitude of the experimental value. Our analysis predicts that σ^* increases with $(U'_0)^3$ the shear, it is observed in [10] that σ^* increases with the shear. Our analysis predicts that λ^* increases with U'_0^{-1} , this is not observed in the experiments where it seems that maximum is independent of the shear.

Second, in the oscillating case, experimentally Rousseaux et al. [6] studied ripples from the rolling ripple stage to the vortex ripple one. The amplitude of the movement is A ($0.01 \text{ m} < A < 0.05 \text{ m}$) and the frequency is f (typically 1 Hz), so that $U_0 = 2A\pi f$ and $\delta = \sqrt{\nu/(\pi f)}$. Then our theory apply for any ε such that equation (14) gives: $\lambda = \varepsilon^3(2A)$: the wave length must be smaller than the amplitude of the movement. It seems to be nearly the case in this experimental setup where the first measured wave length is $\lambda_{initial} \simeq 0.005 \text{ m}$.

Taking $\theta_s = 0.06$, $\phi_s = 30^\circ$, and numerical values from their experiment: $d = 100 \times 10^{-6} \text{ m}$, $s = 2.49$ gives a value

of the most unstable wave length (using Eqs. (30, 34) and Fig. 5):

$$\lambda^* \simeq 0.26 \text{ cm.}$$

The order of magnitude is correct (again we may tune the values). The formula predicts $\lambda^* \propto d^{3/2}$, $\lambda^* \propto \delta^2$, and $\lambda^* \propto \nu^{-1}$. Those are not the scalings of Rousseaux et al. [6] but they obtained that λ^* increases with d , δ and ν^{-1} with different powers. The order of magnitude of time (35) is then about the 0.3 s. which is coherent.

At long time, the Cahn-Hilliard models (Villain-Guillot, and Josserand [52], Bray [34]) predict that $\lambda_{max} \propto \text{Log}(t)$. Rousseaux et al. [6] suggest (but maybe on a too small range of time) this fit for their data. With our model, on a larger range, we instead have a power law. Even if our theory does not strictly compute the separation, the prediction of formula 21 is a good one even when there is flow separation (Lagrée [53]). Our theory is a good approximation of the flow with small separation bubbles. So we model the rolling ripples and the vortex ripple when they are small.

Third, in the decelerated case the observed length is of centimetric size again. There is here a problem because in Caps experiments [13], the size of the grain is not fixed. Taking nevertheless $d = 90 \times 10^{-6}$ m, $\Omega = 0.2 \text{ s}^{-1}$, $R = 0.15$ m, and a typical time scale of 0.05 s (as the experiment is finished in about 2 s) will give an order of magnitude of the ripples of 2 cm which is possible. Unfortunately the dependance in the angular velocity of the wave length is wrong and the time scale of the bed will be of 9 s, which too large.

7 Conclusion

A model for the growth of ripples in a laminar 2D shear flow has been presented. The proposed asymptotical framework is a reinterpretation and generalization of previous studies. It is the natural framework for boundary layer separation. A condition for application is that the height of the created ripples must be smaller than the boundary layer thickness of the basic flow in order to have a basic shear flow.

This shear flow may be steady or slowly varying in time (oscillating or decelerating). A linear solution linking the bed shape and the skin friction is obtained in Fourier space. Depending on the chosen relation linking the transport of sediments and the shear (or skin friction) we obtain a coupled problem. A linear relation with a threshold in shear has been chosen. We present a linear stability analysis of the erodible bed. In the chosen framework, in every case, the bed is unstable for long waves. The instability is due to the fact that the skin friction is in advance of phase with the soil. The short wave length are stabilised by either an “inertial” effect, either a “slope” effect. In the oscillating case, during a period, the bed does not change a lot, this allows a multiscale analysis of the instability. The stabilising effect for the short waves is the same. In the decelerated case, the classical temporal stability analysis has to be changed because the time of the deceleration and the time of growth of the structures must be the same.

Large time simulation of the model equations shows that the ripples merge and we obtain only one bump in the domain (except in the decelerated case because shear is decreasing finally under the threshold). During the coarsening process, the history is independent of the exact value of the parameters. The maximal wave length λ_{max} is proportional to a power of time.

To go further, we should do more refined comparisons between experimental works which are mainly in laminar flows. In fact we need models of transport. To distinguish between an inertia or a slope effect is not a simple task because the two mechanisms (inertia and slope effect) have same global behavior. At small time, short wave numbers are amplified. At large time the coarsening is the same. It would be interesting, but time consuming, to compute the full non linear problem as it is presented here. Finally, to be applicable to reality, instead of looking at perturbations of a linear profile we should look at the perturbations of turbulent flow (a linear and then logarithmic profile).

References

1. NASA, Jet Propulsion Laboratory, <http://www.jpl.nasa.gov/releases/2004/90.cfm>
2. C.T. Yang, (*Mc Graw Hill Education Europe, 1995*) 480
3. J. Fredsøe, R. Deigaard, *Advanced Series on Ocean Engineering* (World Scientific, 1992) **3**, 392
4. P. Nielsen, *Advanced Series on Ocean Engineering* (World Scientific, 1992) **4**, 340
5. M.A. Sherer, F. Melo, M. Marder, *Physics of Fluids* **11** (1), 58 (1999)
6. G. Rousseaux, A. Stegner, J.E. Wesfreid, *Phys. Rev. E* **69**, 031307 (2004)
7. G. Rousseaux, H. Yoshikawa, A. Stegner, J.E. Wesfreid, *Phys. Fluids* **16**, 1049 (2004)
8. F. Charru, H. Mouilleron-Arnould, *J. Fluid Mech.* **452**, 303 (2002)
9. F. Charru, H. Mouilleron-Arnould, O. Eiff, *J. Fluid Mechanics* **519**, 55 (2004)
10. A. Betat, C.A. Kruehle, V. Frette, I. Rehberg, *Eur. Phys. J. E* **8**, 465 (2002)
11. F. Zoueshtiagh, P.J. Thomas, *Phys. Rev.* **61** (5), 5587 (2000)
12. M. Fermigier, P. Jenffer, *Phys Fluids* **14**, S9. (2002)
13. H. Caps, Ph.D. thesis University of Liège.
14. B.C. Barr, D.N. Slinn, *J. Geophys. Res.* **109**, (2004)
15. K.H. Andersen, M.-L. Chabanol, M.V. Hecke, *Phys. Rev. E* **63**, 066308 (2001)
16. K.H. Andersen, J. Fredsøe, *Proceeding of the conference “Coastal Sediments”* (Long Island, 1999)
17. J. Fredsøe, K.H. Andersen, B.M. Sumer, *Coastal Eng.* **38**, 177221 (1999)
18. P. ÊScandura, G. ÊVittori, P. ÊBlondeaux *J. Fluid Mech.* **412**, 355 (2000)
19. T. Loiseleux, P. Gondret, M. Rabaud, D. Doppler, *Phys. Fluids*, submitted
20. A.C. Fowler, in *Geomorphological fluid mechanics*, A. Provenzale, N. Balmforth, pp. 430–454, (Springer-Verlag, Berlin 2001)
21. A. Valance, V. Langlois, *Eur. Phys. J. B* **43**, 283 (2005)

22. C.C. Mei, J. Yue, *Phys. Fluids* **9** (6), 1606 (1997)
23. T. Gerkema, *J. Fluid Mech.* **417**, 303322 (2000)
24. N.L. Komarova, S.J.M.H. Hulsher, *J. Fluid. Mech.* **413**, 219 (2000)
25. B.M. Sumer, M. Bakioglu, *J. Fluid Mech.* **144**, 177 (1984)
26. K.J. Richards, *J. Fluid Mech.* **99**, 597 (1980)
27. B. Andreotti, *JFM* **510**, 47 (2004)
28. A. Valance, F. Rioual, *Eur. Phys. J. B* **10**, 543 (1999)
29. N.J. Balmforth, A. Provenzale, J.A. Whitehead, *The language of pattern and Form in Geomorphological fluid mechanics*, edited by A. Provenzale, N. Balmforth, 3, (Springer-Verlag, Berlin 2001)
30. K. Kroy, G. Sauerma, J. Hermann, *Phys. Rev. Lett.* **88**, 05431 (2002)
31. G. Sauerma, K. Kroy, J. Hermann, *Phys. Rev. Lett.* **64**, 031305 (2001)
32. K.H. Andersen, *Phys. Fluids* **13** (1), 58 (2001)
33. H. Nishimori, M. Yamasaki, K.H. Andersen, *Int. J. Modern Phys. B* **12** (3), 257 (1998)
34. A.J. Bray, *Domain growth and coarsening*, in *Phase Transitions and Relaxation in Systems with Competing Energy Scales*, edited by T. Riste, D. Sherrington, NATO ASI Series C **415**, 405, (Kluwer Academic, 1993)
35. P. du Boys, *Le Rhône et les rivières à lit affouillable*, *J. Annales des Ponts et Chaussées, Série 5*, **18**, 141; (1879) *Etude du régime et de l'action exercée par les eaux sur un lit à fond de graviers indéfiniment affouillable (Study of flow regime and force exerted on a gravel bed of infinite depth)*, *Ann. Ponts et Chaussées, Paris, France, Série 5*, **19**, (in French) 141 (1879)
36. P. Blondeaux, *J. Fluid Mech.* **218**, 1 (1990)
37. B. Andreotti, P. Claudin, P. and S. Douady, *Eur. Phys. J., B* **28**, 341 (2002)
38. H. Schlichting, 7th edn (Mc Graw Hill, New-York, 1987) 748
39. M. Van Dyke, (Parabolic Press, Standford, 1975) 271
40. Darrozès, J.S. *Fluid Dyn. Trans.* **6**, 119 (1971)
41. V. Ya Neiland, *Mekh. Zhid. Gaz.* **4**, 53 (1969)
42. K. Stewartson, P.G. Williams *Proc. Roy. Soc. A* **312**, 181 (1969)
43. F.T. Smith, *IMA J. Appl. Math.* **28**, 207 (1982)
44. V.V. Sychev, A.I. Ruban, V.V. Sychev, G.L. Korolev, (Cambridge U.P., 1998) 352
45. J. Gajjar, F.T. Smith, *Mathematika* **30**, 77 (1983)
46. R.I. Bowles, F.T. Smith, *J.F.M.* **242**, 145 (1992)
47. F.T. Smith, P.W.M. Brighton, P.S. Jackson, J.C.R. Hunt, *J.F.M.* **110**, 1 (1981)
48. K.K.J. Kouakou, P.-Y. Lagrée, submitted
49. K.K.J. Kouakou, H. Caps, P.-Y. Lagrée, *Congrès Français de Mécanique; Nice 01–05 Sept. 2003*
50. W.H. Press, B.P. Flannery, S.A. Teukolsky, W.T. Vetterling, *Numerical Recipes in C: The Art of Scientific Computing*, (Cambridge University Press, 2002)
51. A. Betat, V. Frette, I. Rehberg, *PRL* **83** (1), 88 (1999)
52. S. Villain-Guillot, C. Josserand, *Phys. Rev. E* **66**, 036308 (2002)
53. P.-Y. Lagrée, *Phys. Fluids* **15** (8), 2355 (2003)